MINISTRY OF SUPPLY

AERONAUTICAL RESEARCH COUNCIL
REPORTS AND MEMORANDA

Wind-Tunnel Tests
on a 12-ft Diameter Helicopter Rotor

By
H. B. Squire, R. A. Fail and R. C. W. Eyre

LONDON: HER MAJESTY'S STATIONERY OFFICE

1953

SIX SHILLINGS NET

Wind-Tunnel Tests on a 12-ft Diameter Helicopter Rotor

By

H. B. Squire, R. A. Fail and R. C. W. Eyre

Communicated by the Principal Director of Scientific Research (Air),
Ministry of Supply

Summary.—Measurements of the thrust, torque and flapping angle for a 12-ft diameter rotor over a range of blade angle, shaft inclination and tip-speed ratio have been made to give information on the validity of the standard rotor theory and of the effect of stalling on the retreating blade. Good agreement with the theory was obtained over the normal operating range, using aerofoil characteristics determined from the measurements in the static thrust condition. Stalling was found to be progressive in character showing first by an increase in torque and flapping angle and later by a fall in thrust, as compared with the calculated values.

1. *Introduction.*—Development of helicopters would be considerably assisted by the results of wind-tunnel tests if the necessary technique could be established. Difficulties have been experienced with autorotation tests of small diameter rotors and this has led to doubts as to the reliability of model tests in general. The best way to settle the matter would be to make model tests on a series of rotors of different diameter to establish the range of validity for a given rotor diameter. The experiments on a 12-ft diameter rotor which are described in the present report may, from this point of view, be regarded as one link in this chain; it is hoped to follow them by later tests of a 6-ft diameter rotor.

The other objects of the present tests were to make a comparison with the theory of the rotor developed twenty years ago by Lock[1] and Glauert[2] (*see* also R. & M. 1730[3]) and to establish the limits to the validity of the theory which are imposed by blade stalling. Wind-tunnel tests are preferable for work of this description since the parameters can be varied one by one in a way which is not possible in full-scale testing. Tests of the kind to be described also provide data for some of the aerodynamic derivatives which are important in connection with the calculation of the stability of helicopters.

After some early difficulties (*see* Appendix I) the 12-ft diameter rotor proved satisfactory from the mechanical point of view and the first series of tests was made during the period June to September, 1948. The principal aerodynamic characteristics of the rotor, *viz.*, thrust, torque, and flapping angle, were measured over a wide range of the important parameters, *viz.*, shaft inclination, blade pitch, and tip-speed ratio.

2. *Description of Rotor and Test Equipment.*—2.1. *General.*—The tests were made in the 24-ft Wind Tunnel of the Royal Aircraft Establishment with the rotor on a standard pylon (Fig. 1) so that the lower two-component balance was available for the measurement of aero-dynamic forces. The rotor was driven through a special gearbox by a 25-h.p. d.c. motor

controlled on the Ward-Leonard system. Rotational speed was measured by a 'condenser bridge' operated by a double make-and-break on the rotor shaft. The rotor and other items of special equipment are described in the following sections.

2.2. *Rotor.*—Details of the 12-ft diameter three-bladed rotor are given in Fig. 2. The blades were untwisted and of constant chord (6 in.) and section[7] (NACA 0012). The solidity as defined for helicopter work is the blade area divided by the disk area and equalled 0·0796 for the test rotor. The type of construction shown in Fig. 2 was adopted in order to locate the c.g. of the blade on the quarter-chord line. The hub incorporated flapping and drag hinges with small offsets. Solid friction dampers were found to be necessary on the drag hinges (*see* Appendix I). A worm and wheel were fitted on each blade root to permit fine adjustment of the blade angle, which was measured by means of an inclinometer on a convenient machined flat surface. A similar arrangement was provided to vary the shaft inclination by tilting the entire motor, gearbox and outer casing.

No effort was made to obtain correct tracking of the blades beyond a visual check to ensure that tracking was reasonably good after the blade angles had been set. Previous experience has shown that tracking tends to vary slightly with tip-speed ratio so that if the blades were adjusted to track correctly in the static condition, there could be no guarantee that tracking would remain correct throughout the speed range. Neither of the main disadvantages arising from incorrect tracking, vibration or blurring of the photographs of the disk, was experienced during the present tests.

2.3. *Torque Measurement.*—The motor and gearbox as a unit were mounted on ball-bearings inside a cylindrical steel casing and prevented from rotating by a radial steel spring encastred on the axis of the motor and held between stops on the outer casing. Strain-gauges on the spring were used to measure the torque applied to the rotor. The system was calibrated at frequent intervals by hanging weights from a bar attached to the motor. The electrical circuit is shown in Fig. 3. The two 'live' gauges and the two temperature-compensating gauges were connected locally to form a Wheatstone bridge which was brought into balance by shunting the live gauges. These shunt resistances can conveniently be large enough to render negligible the resistances of the leads which are in series with the shunt resistances. It was found necessary to lag the first few inches of the leads from the bridge with cotton wool, since heat conducted along the wires produced thermo-electric effects at the junctions of the gauge wires and the copper leads.

2.4. *Flapping Angle Measurement.*—The rotor was photographed from the side of the tunnel by means of a remotely controlled F/24 camera and the tilts of the disk were measured from the film. The type of photograph obtained is shown in Fig. 1b. Considerable experiment with lighting and exposure was necessary to produce satisfactory photographs, although in all cases it was possible to measure the coning angle and longitudinal tilt of the disk with reasonable accuracy. At a later stage, however, it was decided to attempt a more complicated analysis of the photographs to determine the lateral tilt, and in many cases the photographs proved to be unsuitable for this. For further tests of this nature, direct measurements at the blade flapping hinge would be desirable.

3. *Method of Test and Presentation of Results.*—The tests were made at 600 r.p.m., giving a tip speed of 377 ft/sec and a tip Reynolds number of $1 \cdot 2 \times 10^6$, with the exception of the higher blade angles in the static condition when rotational speed was limited by the power available. With fixed values of blade angle and shaft inclination, readings of lift, drag and torque were taken at wind speeds of 0, 37·5, 76, 113, 151 and 170 ft/sec corresponding to approximate tip-speed ratios of 0, 0·1, 0·2, 0·3, 0·4, and 0·45. Photographs were also taken in each condition, from which the flapping angles were measured later. The lift and drag readings were corrected for the tare lifts and drags of the rig without rotor and for the rotor weight and resolved to give thrust and horizontal force. The values of the thrust measured on the balance have been corrected for the

2

interference of the pylon and supporting struts, which was determined by measuring the effect of additional structure below the rotor[8].   The correction to the thrust due to this cause amounted to 4·5 per cent.   No tunnel constraint corrections have been applied (see Appendix II).   (To avoid any possible confusion the nomenclature is given in Fig. 4.)

The thrust and torque coefficients and flapping angles were plotted against tip-speed ratio and values read off at standard tip-speed ratios.   This procedure was repeated for shaft inclinations of 0 deg, 5 deg, 10 deg, 15 deg, 20 deg, and 25 deg at blade angles of 4 deg, 8 deg, and 12 deg.   The results for each blade angle were finally plotted against shaft inclination at a series of constant tip-speed ratios and are given in Tables 2 to 5 and Figs. 5 to 6 and 9 to 11.

The use of disk incidence instead of shaft inclination was considered, but as there is little to choose between them, shaft inclination was chosen as it is actually set on the model and not determined from the photographs.   The disk incidence is equal to the shaft inclination minus the flapping angle (Fig. 4 or equation (5)), and the measured values are given in Tables 2 to 5.

Some extra tests over a wider range of blade angle were made to establish the rotor characteristics in the static condition with the rotor axis vertical.   Check tests made with the rotor axis horizontal and the tunnel blocked, showed good agreement.

The flapping angles quoted throughout the present report are defined by the following equation :

$$\beta = a_0 - a_1 \cos \psi - b_1 \sin \psi$$

where β is the blade flapping angle when the position of the blade in azimuth is ψ, measured from the downwind position positive in the direction of rotation, a_1 is the longitudinal flapping angle or backward tilt of the disk, and b_1 is the lateral flapping angle or sideways tilt of the disk.

4. *Formulae Given by Theory.*—The principal objects of the experiments were to decide on the range of validity of tests with the present rotor and to obtain a check on the existing theory of the rotor, which is due essentially to Lock[1] and Glauert[2] (see also R. & M. 1730[3]).   The thrust, torque and flapping angle calculated for infinitely heavy blades by this theory are :—

Thrust Coefficient

$$T_c = \frac{\sigma a}{4}\left[\frac{2}{3}\theta_0\left(\frac{1 - \mu^2 + 2 \cdot 25\mu^4}{1 + 1 \cdot 5\mu^2}\right) - \lambda\left(\frac{1 - 0 \cdot 5\mu^2}{1 + 1 \cdot 5\mu^2}\right)\right] \quad \cdots \quad \cdots \quad \cdots \quad (1)$$

Torque Coefficient

$$Q_c = \frac{\sigma \delta}{8}(1 + \mu^2) + 1 \cdot 05\frac{\sigma a}{4}\lambda\left[\frac{2}{3}\theta_0\left(\frac{1 - 0 \cdot 5\mu^2}{1 + 1 \cdot 5\mu^2}\right) - \lambda\left(\frac{1 + 0 \cdot 5\mu^2}{1 + 1 \cdot 5\mu^2}\right)\right] \quad \cdots \quad (2)$$

Longitudinal Flapping Angle

$$a_1 = \frac{8}{3}\mu\left(\frac{\theta_0 - 0 \cdot 75\lambda}{1 + 1 \cdot 5\mu^2}\right) . \quad \cdots \quad \cdots \quad \cdots \quad \cdots \quad \cdots \quad (3)$$

We also have the formula for the disk incidence i_d

$$\tan i_d = \frac{\lambda}{\mu} - \frac{T_c}{2\mu(\mu^2 + \lambda^2)^{1/2}} \quad \cdots \quad \cdots \quad \cdots \quad \cdots \quad \cdots \quad (4)$$

and the relation between shaft inclination, disk incidence and flapping angle for heavy blades with plain flapping hinges

$$i_s = i_d + a_1 . \quad \cdots \quad \cdots \quad \cdots \quad \cdots \quad \cdots \quad \cdots \quad (5)$$

For given blade angle, shaft inclination and tip-speed ratio, these equations determine the required quantities, provided the aerofoil lift-curve slope, a, and the profile drag coefficient, δ, are known.

A2

The expression for Q_c is made up of a 'profile drag torque coefficient' which depends on δ and an 'induced drag torque coefficient'. The expression given by Lock and Glauert for the induced drag torque has been multiplied by the factor $1 \cdot 05$. This is to make some allowance for non-uniformity of induced velocity over the disk and for the power required for slipstream rotation. The value $1 \cdot 05$ was chosen by consideration on the lines of R. & M. 2521[4] of the probable magnitude of these effects.

The aerofoil section characteristics were determined from the measurements in the static thrust condition, as it would not be justifiable to assume that wind-tunnel data on aerofoils can be used directly. *No allowance for tip loss has been made in calculating the thrust and it is assumed that this effect will be covered by a reduction in aerofoil lift-curve slope.*

5. *Discussion.*—5.1. *Static Thrust and Torque.*—The results of the measurements made at zero forward speed are given in Table 2 and are plotted in Figs. 5 and 6. The rotor was situated about $1 \cdot 2$ rotor diameters above the roof of the balance house and most of the tests were made with the rotor axis vertical. However, some check tests were made with the rotor axis horizontal and the results are given in Table 2. Serious errors can be introduced by the small flow induced in the tunnel circuit by the rotor: this was prevented by hanging a large tarpaulin over the fan some 3 rotor diameters behind the rotor. Satisfactory agreement was then obtained between the two sets of tests, indicating that, with the rotor axis vertical, 'ground effect' was negligible.

The static thrust measurements were taken up to a blade angle of 20 deg at which the blades were fully stalled. The stall was indicated by the falling off of the thrust and also by instability of the blades about their flapping hinges, both of which began at a blade angle of 18 deg. The instability showed itself as an indeterminacy in the flapping angle but was mild in character. This is not suprising as the centrifugal force will prevent any violent angular movements about the flapping hinges even though the normal stability associated with the increase in blade lift with downward flapping is no longer present.

For zero wind speed the formulae (1), (2), (3), and (4) reduce to

$$T_c = \frac{\sigma a}{4}\left(\frac{2}{3}\theta_0 - \lambda\right) \qquad \qquad \qquad \qquad \qquad \qquad (6)$$

$$Q_c = \frac{\sigma \delta}{8} + 1 \cdot 05 \frac{\sigma a}{4} \lambda \left[\frac{2}{3}\theta_0 - \lambda\right] \qquad \qquad \qquad \qquad (7)$$

$$a_1 = 0 \qquad \qquad \qquad \qquad \qquad \qquad \qquad \qquad (8)$$

$$2\lambda^2 = T_c \qquad \qquad \qquad \qquad \qquad \qquad \qquad \qquad (9)$$

and hence,

$$Q_c = \frac{\sigma \delta}{8} + 1 \cdot 05 \frac{T_c^{3/2}}{\sqrt{2}}. \qquad \qquad \qquad \qquad \qquad \qquad (10)$$

It is often convenient to compare static thrust and torque data by means of a static thrust efficiency defined as

$$\eta = \frac{T_c^{3/2}}{\sqrt{2}\,Q_c}. \qquad \qquad \qquad \qquad \qquad \qquad \qquad (11)$$

This quantity is equal to unity if the inflow over the disk is uniform and there are no profile drag or other losses. The values obtained for the present tests are given in Table 2.

A comparison between measured static thrust and the value calculated from equation (6) assuming $a = 5 \cdot 3$, is shown in Fig. 5. This value of the aerofoil lift-curve slope is lower than the usual value of about $5 \cdot 6$, mainly because it includes tip loss effects. The maximum value of the thrust coefficient corresponds to an aerofoil maximum lift coefficient of nearly $1 \cdot 0$.

The profile-drag coefficient of the blade section was obtained from the static thrust and torque measurements using equation (10) as indicated in Fig. 6.

4

The corresponding aerofoil section characteristics obtained from this analysis of the static thrust and torque results are shown in Fig. 7. The rise in profile drag with incidence for propellers is usually more rapid than for wings, but the present profile-drag rise is even more rapid than for propellers. However, the shape of the profile-drag curve for the rotor, when determined in this way, is very sensitive to the factor used to allow for non-uniformity of induced velocity, etc.; the value of $1 \cdot 05$ may therefore be too low.

In applying these results to estimate the thrust and torque with forward speed, the aerofoil lift-curve slope was taken to be $5 \cdot 3$ and no attempt to allow for stalling was made. To avoid a troublesome and uncertain integration over the disk, the profile-drag coefficient was plotted against thrust coefficient for the static condition as shown in Fig. 8. This curve was used to determine the value of δ over the whole range of forward speeds for the calculation of the torque using equation (2).

5.2. *Thrust Coefficient.*—The rotor characteristics for blade angles 4 deg, 8 deg, and 12 deg are plotted in Figs. 9, 10 and 11 respectively. Measured thrust coefficients are shown in Figs. 9a, 10a, and 11a and corresponding calculated curves are provided for comparison in Figs. 9b, 10b, and 11b. The curve of thrust coefficient against shaft inclination for any fixed values of tip-speed ratio and blade angle is approximately a straight line and there are no differences in character between the measured results and the calculations. For blade angles of 4 deg and 8 deg detail agreement between the measurements and calculations is very good. At the blade angle of 12 deg, however, it is apparent that the measured values of the thrust coefficient are smaller than the calculated values for large thrust coefficients. This is due to the onset of the stall on the retreating blade.

5.3. *Torque Coefficient.*—The measured torque coefficients are shown in Figs. 9c, 10c, and 11c for blade angles of 4 deg, 8 deg and 12 deg, respectively. Calculated curves, for comparison, are given in Figs. 9d, 10d and 11d. The calculated torque curves have a maximum value at medium values of shaft inclination (5 deg to 15 deg, depending on the blade angle). At high values of shaft inclination, the torque falls to zero at an inclination slightly greater than that for zero thrust and the rotor is then in the windmilling condition. In this region good agreement exists between the measurements and the calculations. At low (or negative) values of shaft inclination with the thrust coefficient at a high value, the calculated torque again falls to zero and the rotor is said to be in the autorotation condition. At a blade angle of 4 deg (Fig. 9c) there is reasonable agreement with the calculations over the range of tip-speed ratio and shaft inclination covered. At a blade angle of 8 deg (Fig. 10c), however, the torque coefficient remains roughly constant at values of shaft inclination lower than that for maximum torque. At a blade angle of 12 deg (Fig. 11c) in this region the torque coefficient actually increases. The divergence between the calculated and the measured values of the torque which occurs at the smaller shaft inclinations for blade angles of 8 deg and 12 deg is caused by the progressive stalling of the retreating blade, already noticed in connection with the thrust measurements.

5.4. *Flapping Angles and Coning Angle.*—The results of measurements of longitudinal flapping angle (a_1) are plotted in Figs. 9e, 10e and 11e for blade angles of 4 deg, 8 deg and 12 deg, respectively. Calculated curves, for comparison, are given in Figs. 9f, 10f and 11f. Over the range of blade angle tested, there is reasonable agreement between experiment and calculation at a tip-speed ratio of $0 \cdot 1$, but the measured flapping angle increases more rapidly than predicted both with increasing tip-speed ratio and with reduction of shaft inclination. The ratio of measured to calculated flapping angle becomes still greater with the onset of stalling on the retreating blade. This increase in measured flapping angle over the calculated value is in qualitative agreement with German wind-tunnel tests on a double rotor. Also full-scale tests[5] of the C30 autogyro gave a flapping angle 20 per cent greater than the calculated angle. It is possible, however, that the blades in the model were twisting slightly under load.*

---

* Measurements of static thrust were made over a range of rotational speeds and showed very small variations of the thrust coefficient for a range between 200 and 600 r.p.m. for the set of blades used. This is an indication that the twist was probably not serious.

The further increase in flapping angle when stalling begins on the retreating blade is in accordance with later theoretical work[6]. This effect can be simply explained by supposing that the reduction of lift on the retreating blade due to the stall at the tip causes the retreating blade to descend, *i.e.*, to flap more.

Values of the lateral flapping angle (b_1) were derived from the photographs where possible, and the results are given in the Tables 3 and 5.

The coning angle (a_0) was also measured from the photographs and proved to be roughly proportional to the thrust coefficient. This is in accordance with the standard theory which gives for parabolic lift distribution and uniform mass distribution along the blade

$$a_0 = 5 \cdot 9 \ T_c \text{ radians.}$$

The experimental results can be well represented by

$$a_0 = 5 \cdot 4 \ T_c \text{ radians.}$$

5.5. *Force in the Place of the Disk.*—In order to determine the validity of the usual assumption that the force on a rotor is nearly normal to the tip path plane, the forces in the plane of the disk were calculated from the measured values of the lift, drag and flapping angle. It was found that this force was of the order of 1 per cent of the rotor thrust except near the zero thrust condition. The experimental accuracy obtained in these measurements was, therefore, rather low, considerable scatter was evident, and it is not considered worth while to record the results in detail. The results were interesting in one respect, however, in that the force in the plane of the disk was directed forward instead of backward in the condition in which a stall would be expected on the retreating blade. A good example of this phenomenon is given in Fig. 12. A large drag force on the retreating blade represents a forward force in the plane of the disk so that the observed change in sign of the force has a simple explanation.

5.6. *Relation of Model Stalling Indications to Design.*—It is generally recognised that stalling at the tips of the blades is, or will be, an important consideration in helicopter design and operation, but the exact nature of the restriction is still uncertain. Stalling may either (*a*) limit the performance, (*b*) cause an increase in vibration, (*c*) cause the rotor to slow down in case of engine failure, or (*d*) represent an operational boundary in manoeuvres which is not encountered in steady flight. Also, its progressive character with the present model makes the adoption of a simple stalling criterion impracticable. It has, therefore, been decided not to try to draw any definite conclusions about rotor stalling from the present tests. It seems likely, however, that full-scale force measurements on rotors would not be essentially different from the model tests, as the model Reynolds number at the blade tip of $1 \cdot 2 \times 10^6$ is one half of the corresponding full-scale value for many present day helicopters.

6. *Conclusions.*—The measurements are generally in good agreement with calculations based on the standard theory. The major discrepancies between measurements and calculations can be attributed to the effects of stalling of the retreating blade. These effects are not appreciable at a blade angle of 4 deg, but at blade angles of 8 deg and 12 deg, the retreating blade stall is apparent at the higher values of the tip-speed ratio at small shaft inclinations. In these conditions the thrust falls below the calculated value, while the torque and blade flapping are higher than calculated. The divergence is progressive in character and, therefore, no definite limits to design have been deduced from these tests.

REFERENCES

No.	Author	Title, etc.
1	C. N. H. Lock	Further Development of Autogyro Theory. R. & M. 1127. 1927.
2	H. Glauert	On the Horizontal Flight of a Helicopter. R. & M. 1157. 1928.
3	H. B. Squire	The Flight of a Helicopter. R. & M. 1730. 1936.
4	P. Brotherhood	An Investigation in Flight of the Induced Velocity Distribution under a Helicopter Rotor when Hovering. R. & M. 2521. June, 1947.
5	P. A. Hufton and others	General Investigation of the Characteristics of the C.30 Autogyro. R. & M. 1859. 1939.
6	G. J. Sissingh	Jahrbuch der Deutschen Luftfahrtforschung, 1941, I, pp. 351–365.
7	E. N. Jacobs	Tests of Six Symmetrical Airfoils in the Variable Density Wind Tunnel. N.A.C.A. Technical Note No. 385. 1931.
8	R. A. Fail and R. C. W. Eyre	Loss of Static Thrust due to a Fixed Surface under a Helicopter Rotor. A.R.C. Report 12,585. 1949. (Unpublished.)

APPENDIX I

Notes on the Vibrations Encountered

The first rotor made for these tests was fitted with flapping hinges but no drag hinges. When fitted to the original structure, operation was satisfactory up to a moderate wind speed, when a slight vibration was observed. On examination it was found that the blade roots were failing under excessive loads in the drag plane.

A new rotor was, therefore, constructed, incorporating drag hinges and on preliminary runs severe vibrations occurred below the desired rotational speed at zero forward speed.

It was then decided to fit friction dampers on the drag hinges, and in the interval, vibroscope readings were taken at various points on the structure with a small out-of-balance weight on the rotor shaft instead of the rotor. Three main modes of vibration were discovered.

(1) Fore-and-aft oscillations of the motor mass due to bending of the cross tube and main struts (see Fig. 1)—resonant frequency 440 c.p.m.

(2) Vertical oscillations of the motor mass due to bending of the cross tube—resonant frequency 600 c.p.m.

(3) Rotary oscillation of the motor mass in a vertical plane due to flexure of the sting—resonant frequency 600 c.p.m.

It was required to operate the helicopter at 600 r.p.m. and modifications were made to the rig as follows

(i) The fore-and-aft oscillation was allowed to remain substantially unaltered, the slight vibration which occurred while passing through the critical speed being quite acceptable.

(ii) The cross tube was stiffened in the vertical plane by adding the 'king post' type of bracing visible in Fig. 1. The resonant frequency was thus raised well above the required operating speed.

(iii) The flexural stiffness of the sting was reduced by lengthening it, so that the resonant frequency was lowered well below the required operating speed.

With these modifications, and damping on the drag hinges, the helicopter ran very smoothly in all the required test conditions.

APPENDIX II

Tunnel Corrections

The tunnel constraint correction for a wing is

$$\Delta\alpha = -\frac{1}{8}\frac{S}{C}C_L$$

in the usual notation where S is the wing area, C is the area of tunnel cross-section, and C_L is the lift coefficient. For an open-jet wind tunnel the effective incidence is less than the geometrical incidence by $\Delta\alpha$.

For the 12-ft diameter rotor in a 24-ft wind tunnel we have $S/C = \frac{1}{4}$ and also $C_L = 2T_c\mu^2\sec^2 i_s$ so that

$$\Delta i_s = \frac{1}{16}\frac{T_c}{\mu^2\sec^2 i_s}\cdot$$

The sign of the correction is such as to increase the shaft inclination i_s by Δi_s. For $\mu = 0\cdot3$ the highest value of Δi_s for the measured values of T_c is $0\cdot4$ deg which is just significant. For $\mu = 0\cdot1$ the maximum value of the correction is 3 deg.

The corrections, if applied, tend to improve the agreement between calculation and measurement. As their validity is rather uncertain they have not been applied but the values of the corrections to the geometrical shaft inclination are given in Tables 3, 4, and 5.

The absence of any correction in the static thrust condition ($\mu = 0$) has already been noted.

TABLE 1

List of Symbols and Leading Dimensions

R	Radius of rotor	$= 6\cdot00$ ft
c	Chord of blades	$= 0\cdot500$ ft
N	Number of blades	$= 3$
σ	Solidity of rotor $= Nc/\pi R$	$= 0\cdot0796$
θ_0	Blade angle (deg)	
i_s	Shaft inclination (deg)	
i_d	Disk incidence (incidence of tip-path plane)	
a_0	Coning angle (deg)	
a_1	Longitudinal flapping angle (deg)	
b_1	Lateral flapping angle (deg)	
Ω	Angular velocity of rotor (radn/sec)	
V	Tunnel speed (ft/sec)	
u	Component velocity of air at rotor disc parallel to shaft	
T	Thrust (lb)	
Q	Torque (lb/ft)	
μ	Tip-speed ratio $= V\cos i_s/\Omega z$	
λ	$\mu/\Omega R$	
a	Slope of lift curve of blade section	
δ	Mean profile-drag coefficient of blade section	
T_c	Thrust coefficient $\quad= T/\rho\Omega^2 R^2\pi R^2$	
Q_c	Torque coefficient $\quad= Q/\rho\Omega^2 R^3\pi R^2$	
η	Static-thrust efficiency $= T_c^{3/2}/\sqrt{2}Q_c$	

TABLE 2

Static Thrust and Torque

θ (deg)	$10^3 T_c$	$10^3 Q_c$	η	Remarks
1	0·17	0·079	0·019	
4	1·56	0·129	0·339	Mean of values obtained through-
8	4·42	0·336	0·617	out the course of the tests.
12	7·97	0·716	0·703	
13	8·80	0·853	0·672	
14	10·35	0·983	0·755	
15	10·78	1·123	0·701	
16	11·03	1·263	0·646	
17	12·08	1·396	0·668	
18	12·49	1·55	0·635	Instability of blade motion starts
19	12·61	2·10	0·476	Increasing
20	11·71	2·47	0·363	Amplitude 6 in. at tips
8	4·54	0·346	0·624	Check points obtained with rotor
12	7·88	0·727	0·680	axis horizontal.

TABLE 3

Rotor Characteristics : $\theta_0 = 4$ deg

μ	i_s (deg)	Δi_s (deg)	i_d (deg)	a_1 (deg)	b_1 (deg)	$10^3 T_c$	$10^3 Q_c$
0	—	—	—	0	0	1·56	0·129
	0	1·1	− 1·1	1·1	2·2	3·08	0·139
	5	0·8	+ 4·0	1·0	0·8	2·46	0·135
	10	0·6	9·2	0·8	0·1	1·85	0·134
0·1	15	0·4	14·3	0·7	0·1	1·36	0·126
	20	0·2	19·5	0·5	0·2	0·80	0·112
	25	0	24·5	0·5	0·7	0·18	0·086
	0	0·4	− 2·4	2·4	1·1	4·25	0·122
	5	0·2	+ 3·1	1·9	0·3	2·58	0·137
0·2	10	0·1	8·3	1·7	0·2	1·11	0·123
	15	0	14·0	1·0	0·4	−0·47	0·063
	0	0·2	− 4·5	4·5	1·4	5·21	0·074
	2·5	0·2	− 1·7	4·2	0·5	4·00	0·112
0·3	5	0·1	+ 1·7	3·3	0	2·70	0·135
	7·5	0	4·9	2·6	0·2	1·29	0·130
	10	0	8·1	1·9	0·4	0·03	0·091
	0	0·1	− 6·7	6·7	1·4	5·67	0·042
	2·5	0·1	− 2·8	5·3	0·8	4·16	0·090
0·4	5	0	+ 1·2	3·8	0	2·21	0·134
	7·5	0	5·1	2·4	−0·1	0·34	0·106
	0	0·1	− 8·1	8·1	1·5	6·40	0·017
0·45	2·5	0·1	3·3	6·3	1·0	4·61	0·073
	5·0	0	+ 0·2	4·8	−0·1	2·26	0·131

9

TABLE 4

Rotor Characteristics : $\theta_0 = 8$ deg

μ	i_s (deg)	Δi_s (deg)	i_d (deg)	a_1 (deg)	b_1 (deg)	$10^3 T_c$	$10^3 Q_c$
0	—	—	—	0	—	4·42	0·336
	0	2·1	− 2·1	2·1	—	6·16	0·326
	5	1·9	+ 3·2	1·8	—	5·53	0·329
0·1	10	1·7	8·1	1·9	—	5·00	0·336
	15	1·4	13·2	1·8	—	4·41	0·330
	20	1·2	18·2	1·8	—	3·95	0·322
	25	1·0	23·5	1·5	—	3·11	0·288
	0	0·7	− 4·8	4·8	—	8·16	0·320
	5	0·6	+ 0·8	4·2	—	6·61	0·298
0·2	10	0·4	6·3	3·7	—	4·97	0·324
	15	0·3	11·5	3·5	—	3·46	0·305
	20	0·1	17·5	2·5	—	2·01	0·233
	25	0	23·0	2·0	—	0·33	0·110
	0	0·3	− 9·2	9·2	—	9·04	0·315
	5	0·3	− 2·1	7·1	—	6·96	0·280
0·3	10	0·2	+ 4·0	6·0	—	4·51	0·298
	15	0·1	10·3	4·7	—	2·08	0·251
	20	0	16·5	3·5	—	−0·76	0·042
	0	0·2	−11·7	11·7	—	9·91	0·302
0·4	5	0·1	− 4·0	9·0	—	6·79	0·287
	10	0·1	+ 3·5	6·5	—	3·52	0·275
	15	0	10·1	4·9	—	0·31	0·115
	5	0·1	− 5·8	10·8	—	7·29	0·260
0·45	10	0·1	+ 1·7	8·3	—	3·53	0·254
	15	0	10·9	4·1	—	−0·46	0·036

10

TABLE 5

Rotor Characteristics : $\theta_0 = 12$ deg

μ	i_s (deg)	Δi_s (deg)	i_d (deg)	a_1 (deg)	b_1 (deg)	$10^3 T_c$	$10^3 Q_c$
0	—	—	—	0	0	7·97	0·716
	0	3·1	− 3·9	3·9	3·5	9·08	0·680
	5	3·0	+ 0·5	4·5	3·3	8·67	0·676
0·1	10	2·8	7·6	2·4	2·5	8·42	0·676
	15	2·6	11·9	3·1	2·0	8·00	0·689
	20	2·3	16·8	3·2	1·2	7·51	0·665
	25	1·9	22·2	2·8	0·4	5·69	0·650
	0	0·9	−10·2	10·2	4·8	11·14	0·769
	5	0·8	−3·7	8·7	3·9	9·95	0·688
0·2	10	0·7	+ 2·4	7·6	2·6	8·73	0·644
	15	0·6	8·7	6·3	1·6	7·73	0·639
	20	0·5	14·9	5·1	0·6	6·21	0·608
	25	0·3	20·2	4·8	−0·3	4·62	0·538
	5	0·4	− 8·9	13·9	4·7	10·81	0·777
	10	0·3	− 1·9	11·9	3·0	8·90	0·669
0·3	15	0·2	+ 6·1	8·9	1·3	6·90	0·558
	20	0·1	+13·0	7·0	0	4·35	0·511
	25	0	19·2	5·8	−0·9	1·86	0·29
	10	0·2	− 3·0	13·0	3·1	8·82	0·707
0·4	15	0·1	+ 4·7	10·3	0·9	5·75	0·512
	20	0	12·3	7·7	0	2·33	0·339
	25	0	19·8	5·2	−0·4	−1·39	−0·22
0·45	15	0·1	3·5	11·5	1·6	5·12	0·482
	20	0	12·0	8·0	−0·2	1·33	0·237
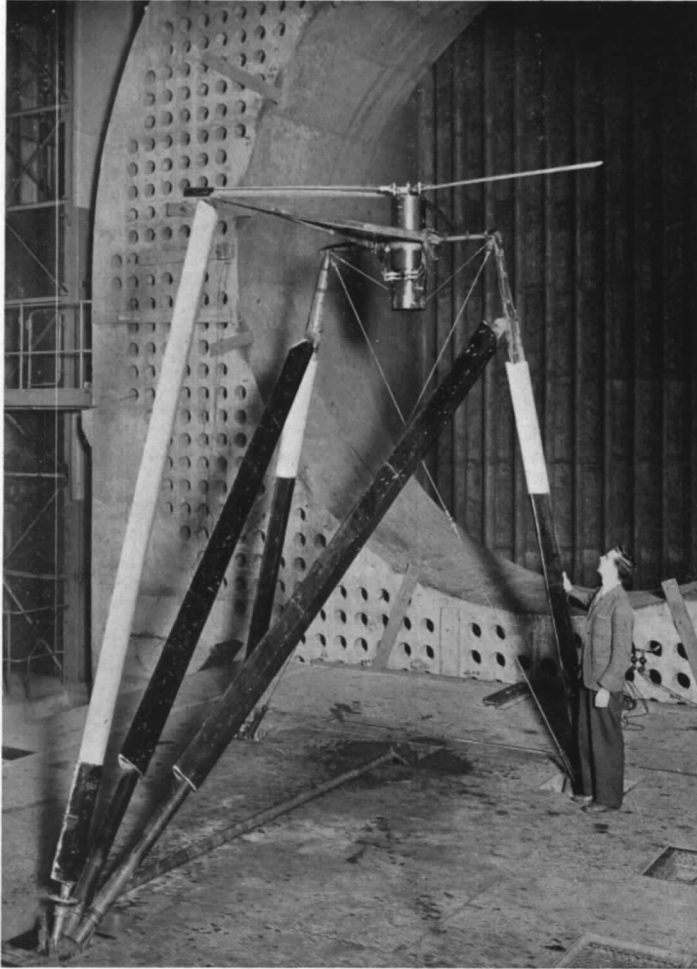
(a) General View.

(b) Side View.

FIG. 1. 12-ft diameter rotor in 24-ft wind tunnel.
$\theta_o = 8$ deg, $i_s = 15$ deg, $\mu = 0 \cdot 3$.

6" CHORD

NACA 0012

BRASS

TEAK

PINE

TIP SHAPE IN PLAN
VIEW AS BLADE
SECTION PROFILE

0·72"

RAD.

A

A

5' 5"

6' 0"

LEADING EDGE

WORM & WHEEL
FOR PITCH
VARIATION

3·0"

RAD.

FRICTION
DAMPER

DRAG HINGE

4·75"

2·25"

FLAPPING HINGE

C/L OF ROTOR
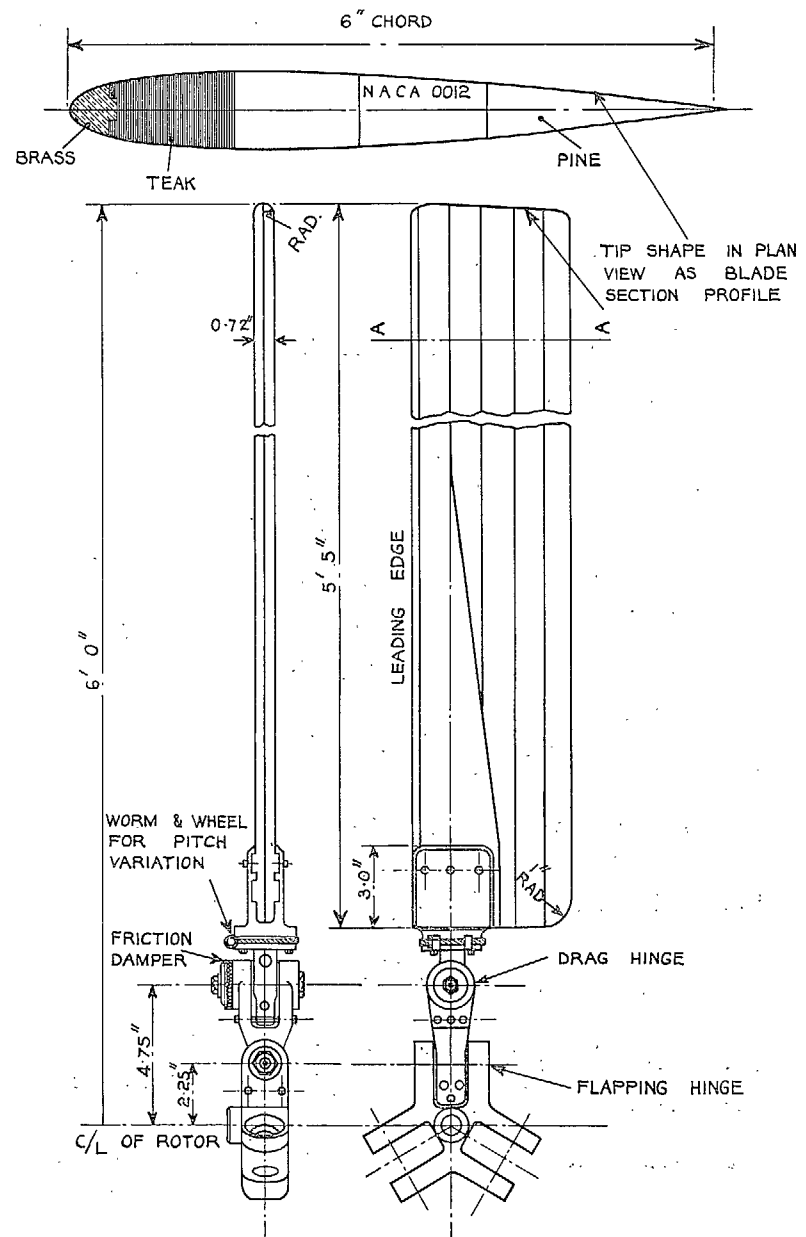
Fig. 2.   Details of 12-ft diameter rotor.

TEMPERATURE
COMPENSATING GAUGES

'LIVE' GAUGES

5-CORE CABLE

VERNIER POTENTIOMETER
USED TO BALANCE BRIDGE

SENSITIVE
GALVANOMETER

RESISTANCES

2 V ACCUMULATOR
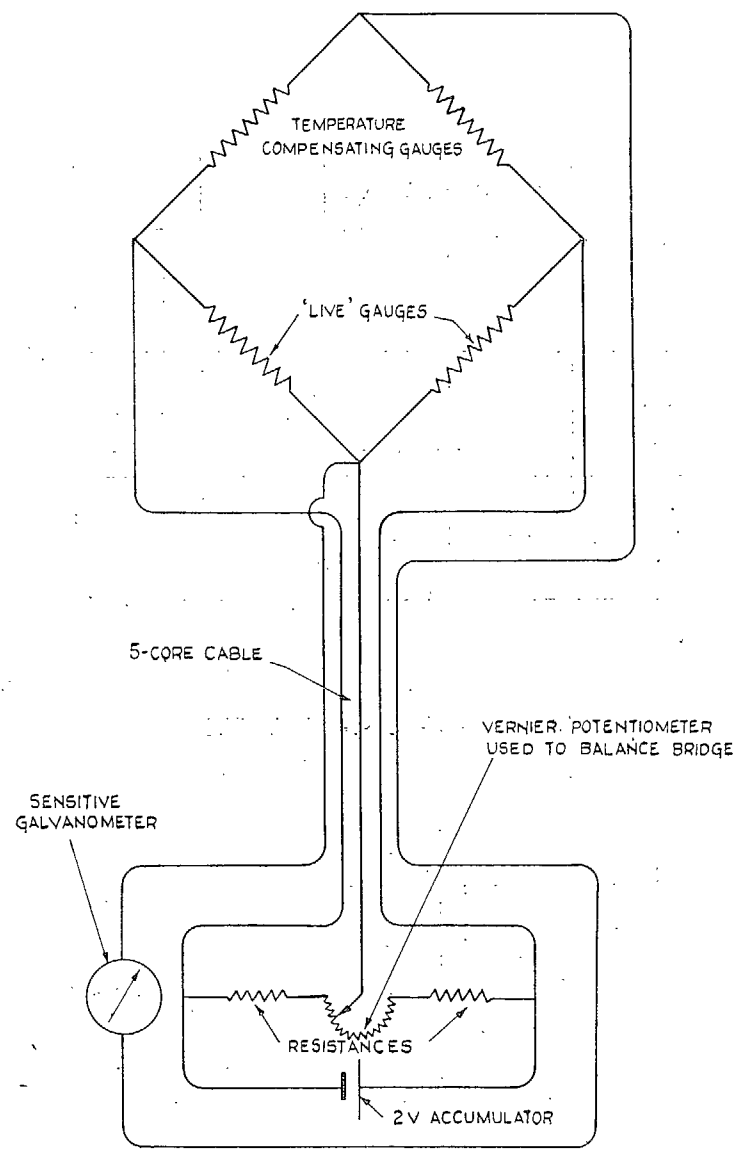
Fig. 3.   Diagram of strain-gauge bridge circuit used for
torque measurement.
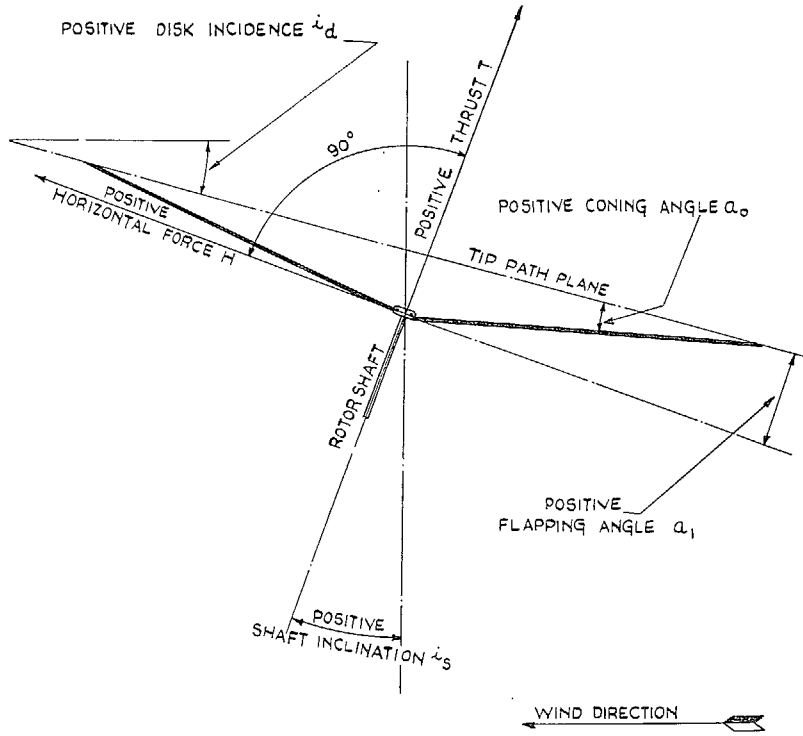
FIG. 4. Nomenclature diagram.
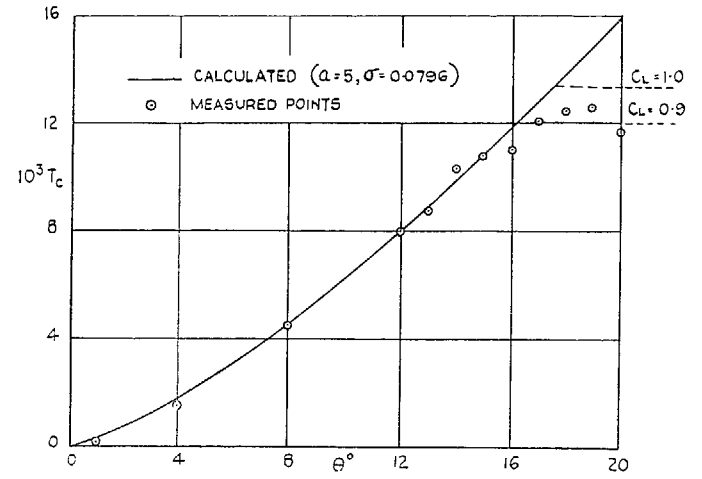
FIG. 5. Static thrust coefficient.
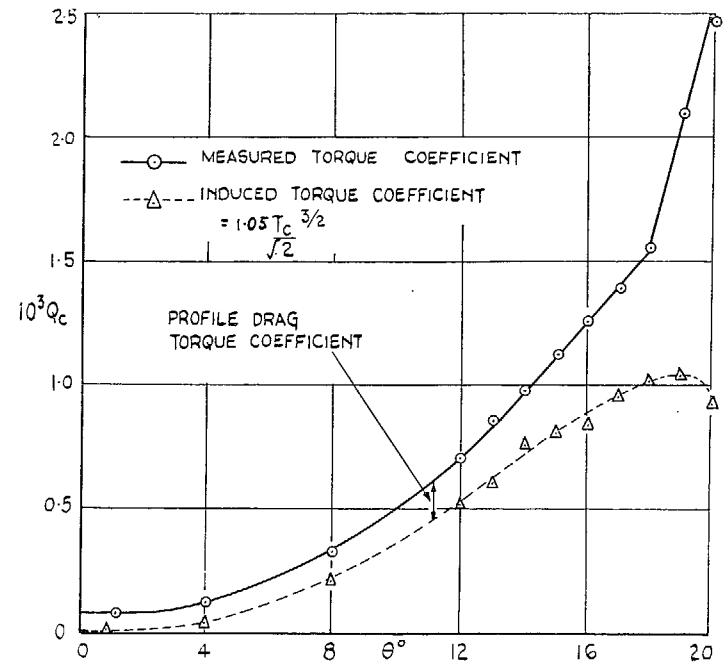
FIG. 6. Static torque coefficient.
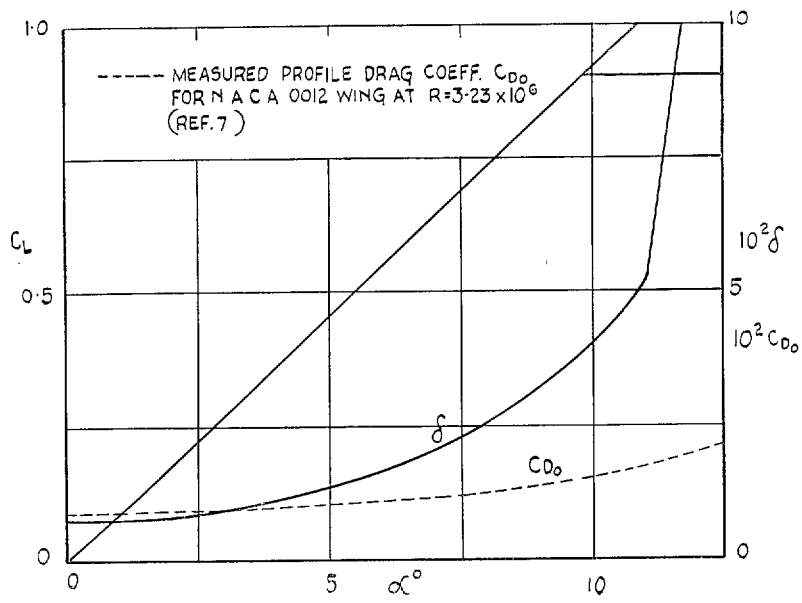
FIG. 7.
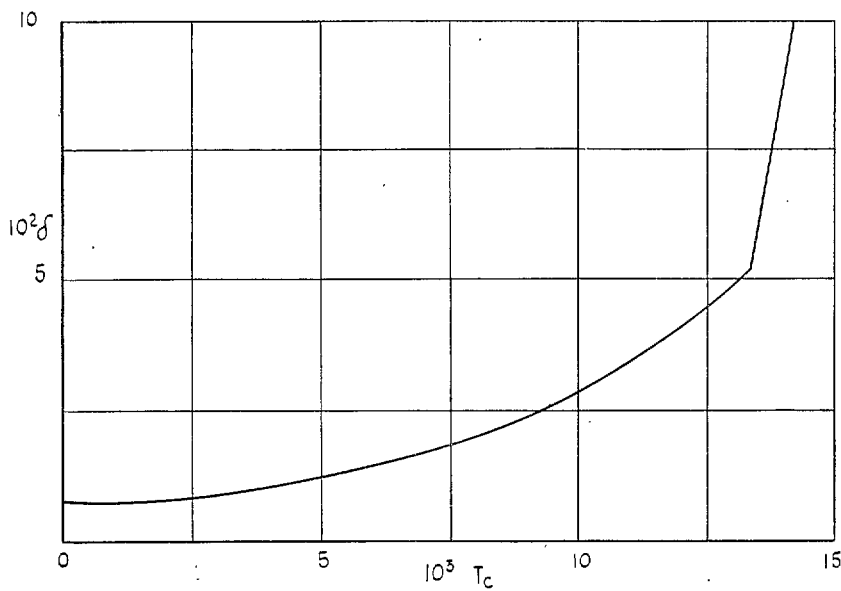
FIG. 8.

FIGS. 7 and 8.   Mean blade characteristics used in calculations.   Deduced from measured thrust and torque.

15

$10^3 T_c$

$\mu = 0$

$\mu = 0.1$

$\mu = 0.2$

$\mu = 0.3$

$\mu = 0.4$

$\mu = 0.45$

λ_s°
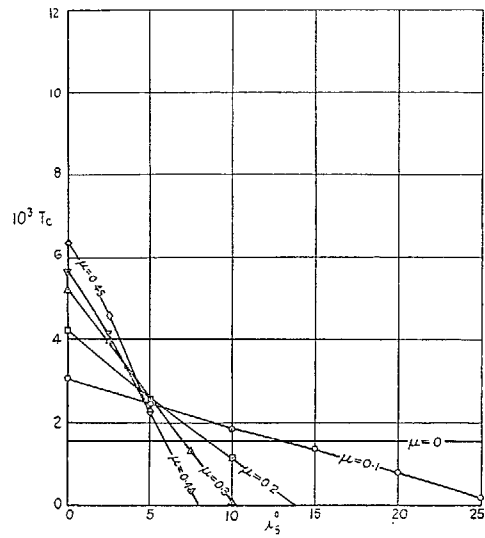
FIG. 9a. Measured thrust.

$10^3 Q_c$

$\mu = 0$

$\mu = 0.1$

$\mu = 0.2$

$\mu = 0.3$

$\mu = 0.4$

$\mu = 0.45$

λ_s°
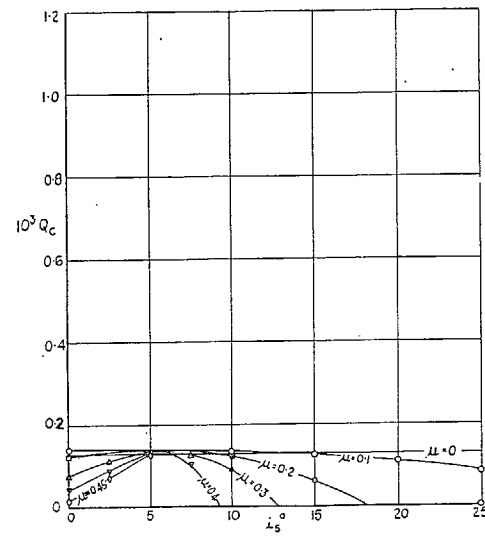
FIG. 9c. Measured torque.

a_1°

$\mu = 0.45$

$\mu = 0.4$

$\mu = 0.3$

$\mu = 0.2$

$\mu = 0.1$

λ_s°
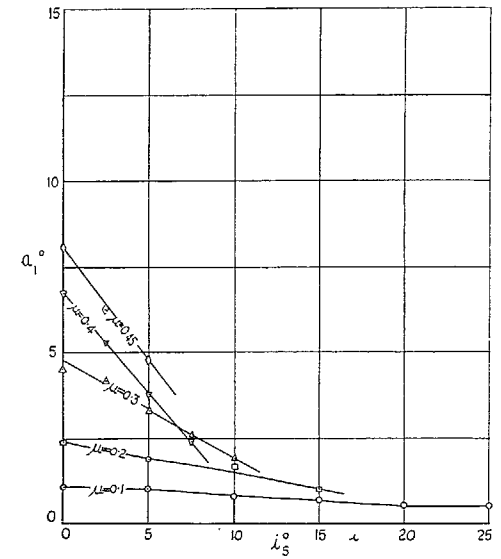
FIG. 9e. Measured flapping angle.

$10^3 T_c$

$\mu = 0$

$\mu = 0.1$

$\mu = 0.2$

$\mu = 0.3$

$\mu = 0.4$

$\mu = 0.45$

λ_s°
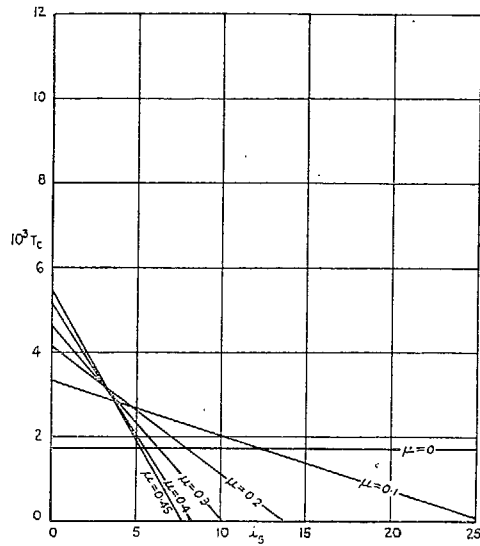
FIG. 9b. Calculated thrust.

$10^3 Q_c$

$\mu = 0$

$\mu = 0.1$

$\mu = 0.2$

$\mu = 0.3$

$\mu = 0.4$

$\mu = 0.45$

λ_s°
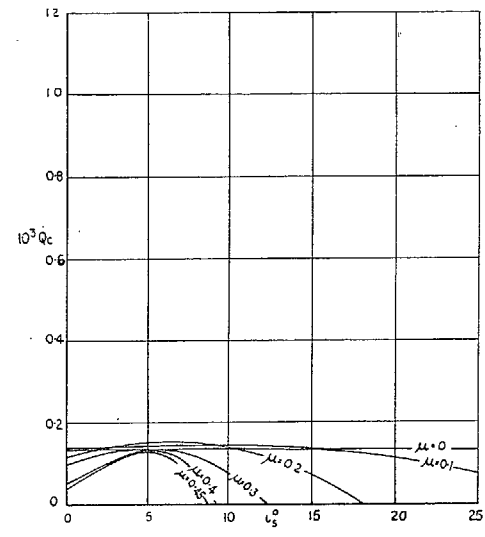
FIG. 9d. Calculated torque.

a_1°

$\mu = 0.45$

$\mu = 0.4$

$\mu = 0.3$

$\mu = 0.2$

$\mu = 0.1$

λ_s°
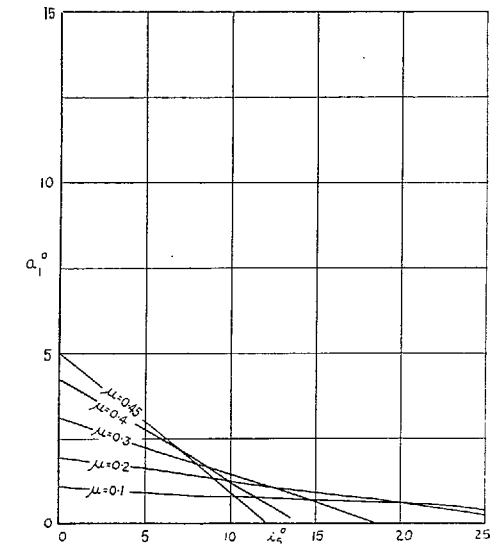
FIG. 9f. Calculated flapping angle.

FIG. 9.   12-ft rotor.   Blade angle 4 deg.
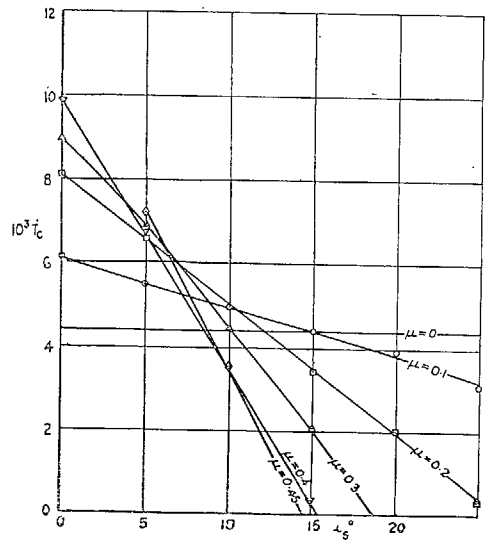
FIG. 10a. Measured thrust.
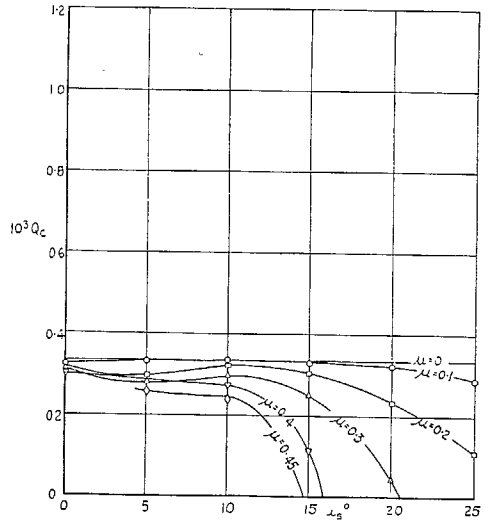
FIG. 10c. Measured torque.
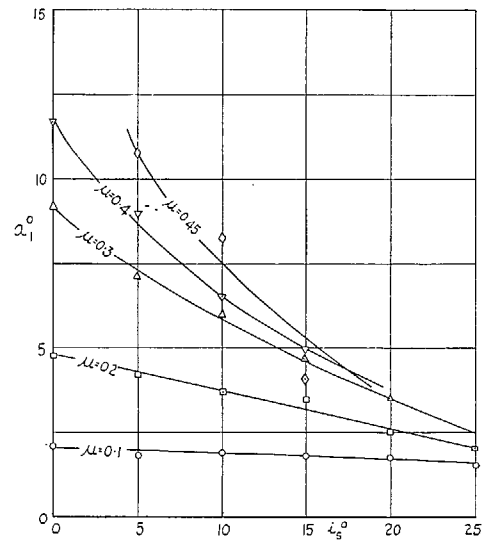
FIG. 10e. Measured flapping angle.
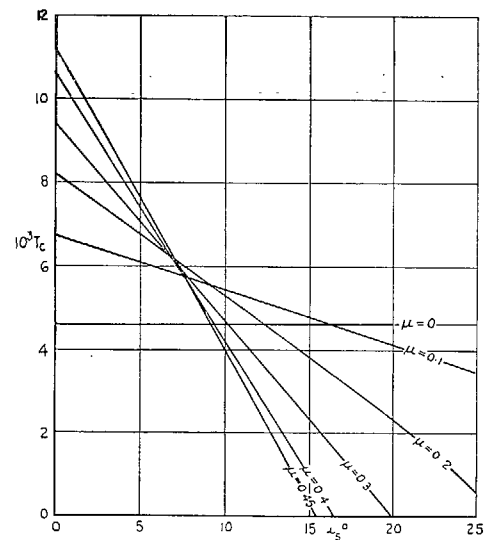
FIG. 10b. Calculated thrust.
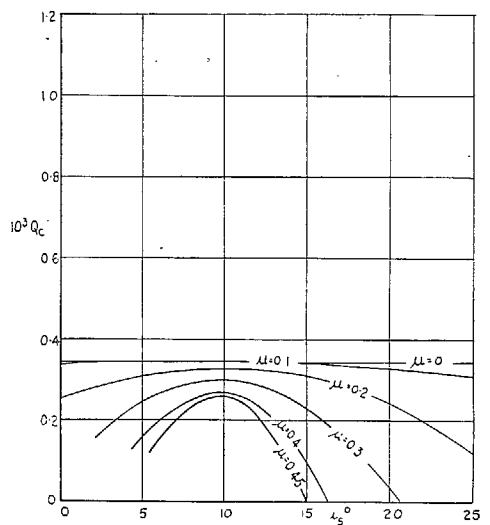
FIG. 10d. Calculated torque.
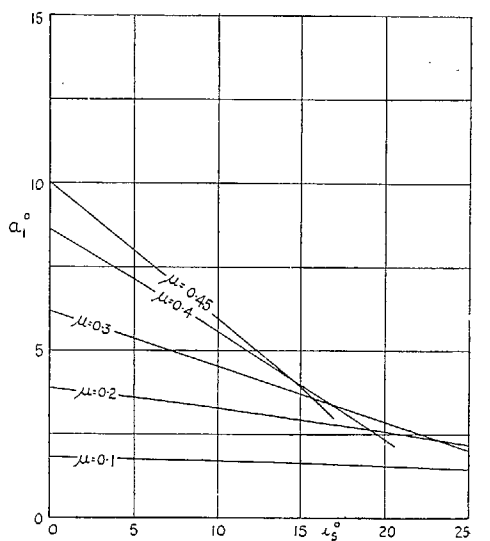
FIG. 10f. Calculated flapping angle.

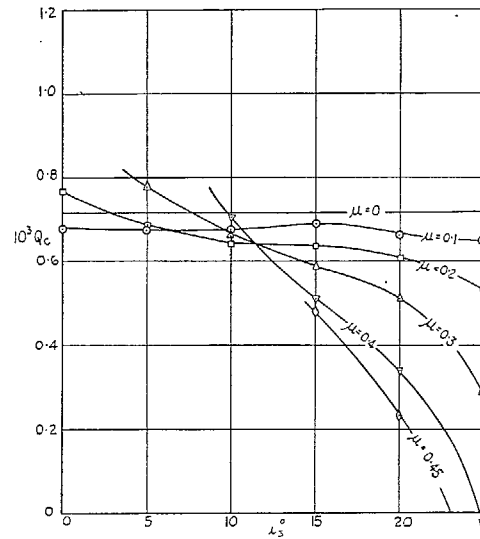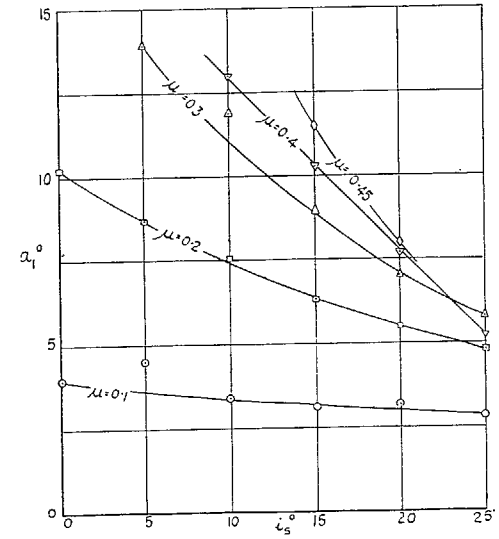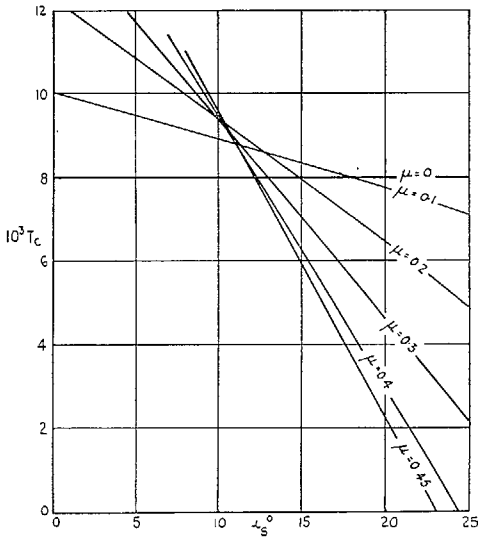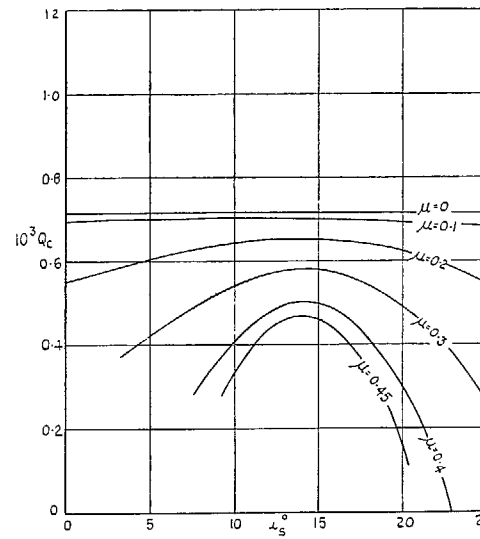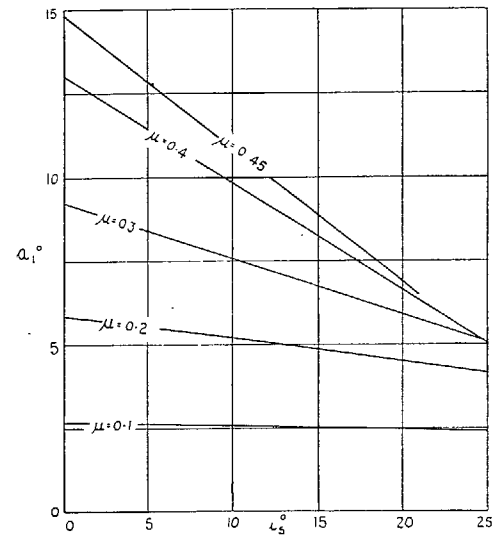FIG. 10. 12-ft rotor. Blade angle 8 deg.
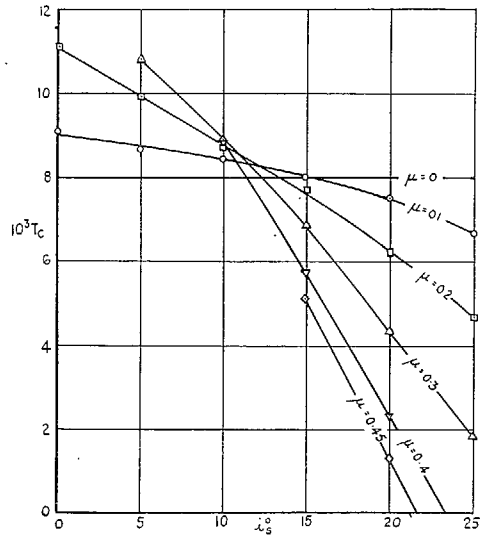
FIG. 11a. Measured thrust.

FIG. 11c. Measured torque.

FIG. 11e. Measured flapping angle.

FIG. 11b. Calculated thrust.

FIG. 11d. Calculated torque.

FIG. 11f. Calculated flapping angle.
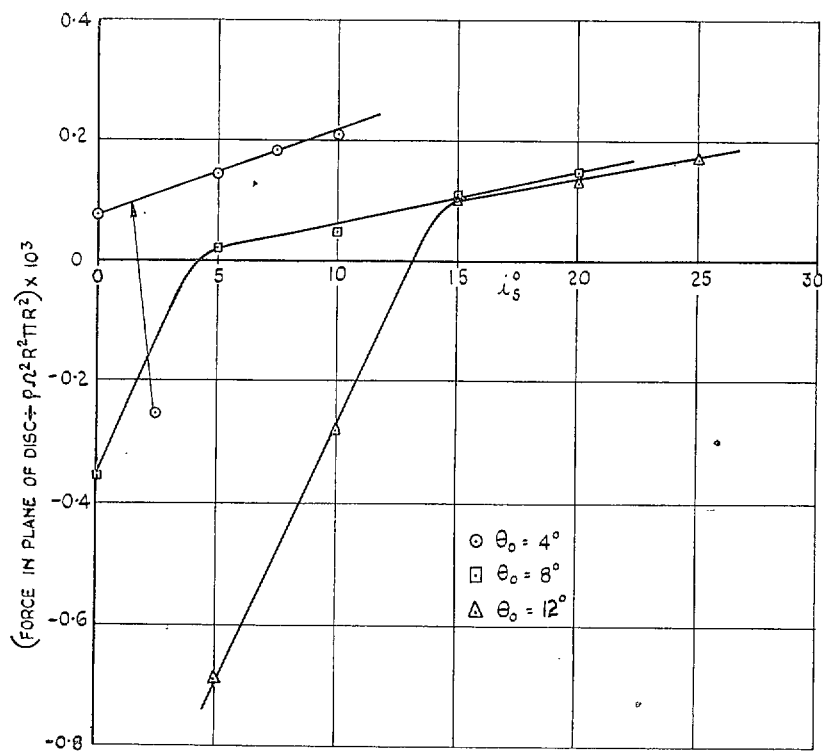
FIG. 11. 12-ft rotor. Blade angle 12 deg.

FIG. 12. Force in plane of rotor disc. ($\mu = 0 \cdot 3$.)

Publications of the
Aeronautical Research Council

ANNUAL TECHNICAL REPORTS OF THE AERONAUTICAL RESEARCH COUNCIL (BOUND VOLUMES)

1936 Vol. I. Aerodynamics General, Performance, Airscrews, Flutter and Spinning. 40s. (40s. 9d.)
   Vol. II. Stability and Control, Structures, Seaplanes, Engines, etc. 50s. (50s. 10d.)

1937 Vol. I. Aerodynamics General, Performance, Airscrews, Flutter and Spinning. 40s. (40s. 10d.)
   Vol. II. Stability and Control, Structures, Seaplanes, Engines, etc. 60s. (61s.)

1938 Vol. I. Aerodynamics General, Performance, Airscrews. 50s. (51s.)
   Vol. II. Stability and Control, Flutter, Structures, Seaplanes, Wind Tunnels, Materials. 30s.
      (30s. 9d.)

1939 Vol. I. Aerodynamics General, Performance, Airscrews, Engines. 50s. (50s. 11d.)
   Vol. II. Stability and Control, Flutter and Vibration, Instruments, Structures, Seaplanes, etc.
      63s. (64s. 2d.)

1940 Aero and Hydrodynamics, Aerofoils, Airscrews, Engines, Flutter, Icing, Stability and Control,
      Structures, and a miscellaneous section. 50s. (51s.)

1941 Aero and Hydrodynamics, Aerofoils, Airscrews, Engines, Flutter, Stability and Control,
      Structures. 63s. (64s. 2d.)

1942 Vol. I. Aero and Hydrodynamics, Aerofoils, Airscrews, Engines. 75s. (76s. 3d.)
   Vol. II. Noise, Parachutes, Stability and Control, Structures, Vibration, Wind Tunnels
      47s. 6d. (48s. 5d.)

1943 Vol. I. (In the press.)
   Vol. II. (In the press.)

ANNUAL REPORTS OF THE AERONAUTICAL RESEARCH COUNCIL—

1933-34	1s. 6d. (1s. 8d.)	1937	2s. (2s. 2d.)
1934-35	1s. 6d. (1s. 8d.)	1938	1s. 6d. (1s. 8d.)
April 1, 1935 to Dec. 31, 1936.	4s. (4s. 4d.)	1939-48	3s. (3s. 2d.)

INDEX TO ALL REPORTS AND MEMORANDA PUBLISHED IN THE ANNUAL TECHNICAL REPORTS, AND SEPARATELY—

April, 1950 - - - - R. & M. No. 2600. 2s. 6d. (2s. 7½d.)

AUTHOR INDEX TO ALL REPORTS AND MEMORANDA OF THE AERONAUTICAL RESEARCH COUNCIL—

1909-1949. R. & M. No. 2570. 15s. (15s. 3d.)

INDEXES TO THE TECHNICAL REPORTS OF THE AERONAUTICAL RESEARCH COUNCIL—

December 1, 1936 — June 30, 1939.	R. & M. No. 1850.	1s. 3d. (1s. 4½d.)
July 1, 1939 — June 30, 1945.	R. & M. No. 1950.	1s. (1s. 1½d.)
July 1, 1945 — June 30, 1946.	R. & M. No. 2050.	1s. (1s. 1½d.)
July 1, 1946 — December 31, 1946.	R. & M. No. 2150.	1s. 3d. (1s. 4½d.)
January 1, 1947 — June 30, 1947.	R. & M. No. 2250.	1s. 3d (1s. 4½d.)
July, 1951.	R. & M. No. 2350.	1s. 9d. (1s. 10½d.)

Prices in brackets include postage.

Obtainable from

HER MAJESTY'S STATIONERY OFFICE